Electronic Supporting Information Available

Controlling emitting dipole orientations by N^O-ancillary electronic effects of [Ir(C^N)$_2$(N^O)]-heteroleptic Ir(III)-complexes towards efficient near-infrared (NIR) polymer light-emitting diodes (PLEDs)

Siyu Hou,‡[a] Jiaxiang Liu,‡[a] Baowen Wang,[a] Tiezheng Miao,[a] Xingqiang Lü,[a,*] Wentao Li,[a,*] Guorui Fu,[a,c] Weixu Feng[b,*] and Wai-Yeung Wong[c,*]

Supporting information

Materials and characterization

All reagents were received from Sigma Aldrich and used without further purification. All solvents unless otherwise stated were degassed and stored over 3 Å activated molecular sieves prior to use. All manipulations of air and water sensitive compounds were carried out under dry N_2 using the standard Schlenk line techniques.

Elemental analysis (EA) was performed on a Perkin-Elmer 240C elemental analyzer. Fourier Transform Infrared (FT-IR) spectra were recorded on a Nicolet Nagna-IR 550 spectrophotometer in the region 4000-400 cm^{-1} using KBr pellets. ^1H NMR spectra were recorded on a JEOL EX 400 spectrometer with $SiMe_4$ as internal standard in $CDCl_3$ or DMSO-

d_6 at room temperature. ^{1}H NMR and ^{13}C NMR spectra were recorded on a JEOL EX 400 spectrometer and a Bruker Advance-III FT-NMR spectrometer with $SiMe_4$ as internal standard in $CDCl_3$ at room temperature, respectively. Electro-spray ionization mass spectrometry (ESI-MS) was performed on a Finnigan LCQ^{DECA} XP HPLC-MS_n mass spectrometer with a mass to charge (*m/z*) range of 4000 using a standard electro-spray ion source and CH_2Cl_2 as the solvent. Electronic absorption spectra in the UV-visible-NIR region were recorded with a Cary 300 UV spectrophotometer. Visible or NIR emission and excitation spectra were collected by a combined fluorescence lifetime and steady-state spectrometer (FLS-980, Edinburgh) with a 450 W Xe lamp. Excited-state decay times were obtained by the same spectrometer but with a μF900 Xe lamp. The quantum yield (Φ_{PL}) in solution was measured with free-base tetraphenylporphyrin (Φ_r = 0.13 in toluene solution at 298 K) as the standard.[1] The solution was degassed by three freeze-pump-thaw circles. The following equation 1 was used to calculate the quantum yields:

$$\Phi_s = \Phi_r \times [(n_s^2 \times A_r \times I_s)/(n_r^2 \times A_s \times I_r)] \qquad (1)$$

where Φ_s is the quantum yield of the sample, Φ_r is the quantum yield of the reference, n_s is the refractive index of the sample, n_r is the refractive index of the reference, A_s and A_r are the absorbance of the sample and the reference at the wavelength of excitation (355 nm), respectively, and the I_s and I_r are the integrated areas of emission bands of the sample and the reference from 600 to 900 nm, which were recorded by a red photomultiplier tube (PMT) detector. Thermal properties were characterized using thermogravimetric (TG) analyses on a NETZSCH TG 209 instrument under a flow of nitrogen at a heating rate of 10 °C/min. Powder X-ray diffraction (PXRD) patterns were recorded on a D/Max-IIIA

diffractometer with graphite-monochromatized Cu Kα radiation (λ = 1.5418 Å). The atomic force microscopy (AFM) images were measured on a NT-MDT Atomic Force Microscope NEXT.

Synthesis of the C^N ligand Hiqbt (1-(benzo[b]-thiophen-2-yl)-isoquinoline)

The C^N ligand **Hiqbt** was synthesized from the improved Suzuki coupling reaction of 2-chloro-isoquinoline[2] (instead of 2-bromo-isoquinoline[3]) with benzo[*b*]thien-2-yl boronic acid. A mixture of 2-chloro-isoquinoline (0.653 g, 4.0 mmol) and benzo[*b*]thien-2-y boronic acid (0.713 g, 4.0 mmol) was dissolved into absolute mixed solvents of toluene-EtOH (60 mL; v/v = 2:1) under a N_2 atmosphere. Then an aqueous solution (20 mL) of Na_2CO_3 (2 M) was added, and the mixture was degassed by a N_2 flow. Anhydrous $Pd(PPh_3)_4$ (190 mg, 0.2 mmol; 5 mol%) was added to the reaction mixture which was then heated at 85 °C for 48 h. The complete consumption of reagents was monitored by thin-layer chromatography (Hexane/AcOEt, v/v = 9:1). After cooling to room temperature, the organic phase was washed with brine and extracted with absolute CH_2Cl_2 (3×20 mL) three times. The combined organic phase was dried over anhydrous Na_2SO_4, and further purified with flash-column chromatography on silica gel (Hexane/AcOEt, v/v = 9:1), affording an off-white solid. Yield: 0.762 g (73%). Calcd for $C_{17}H_{11}NS$: C, 78.13; H, 4.24; N, 5.36%. Found: C, 78.05; H, 4.36; N, 5.29%. ^{1}H NMR (400 MHz, DMSO-d_6): δ (ppm) 8.70 (d, 1H, -Py), 8.61 (d, 1H, -Ph), 8.19 (s, 1H, -Th), 8.11 (d, 1H, -Ph), 8.06 (m, 1H, -Ph), 8.02 (m, 1H, -Py), 7.88 (m, 2H, -Ph), 7.81 (m, 1H, -Ph), 7.46 (m, 2H, -Ph).

Synthesis of chloride-bridged dimer intermediate $[Ir(iqbt)_2(\mu\text{-}Cl)]_2$

The chloride-bridged dimer intermediate $[Ir(iqbt)_2(\mu\text{-}Cl)]_2$ was synthesized according to an improved Nonoyama procedure[4] and used directly for the next step without further purification. To a mixed solvents of 2-ethoxyethanol and D. I. water (V/V = 3:1, 24 mL), **Hiqbt** (400 mg, 2.6 mmol) and $IrCl_3 \cdot 3H_2O$ (208 mg, 1.2 mmol) were added, and the resultant mixture was heated overnight at 110 °C under a N_2 atmosphere. After cooling to RT, a saturate aqueous solution of NaCl (25 mL) was added and the dark-brown suspension was filtered. The brown solid products were further washed with D. I. water, diethyl ether and hexane, and dried at 45 °C under vacuum to constant weight. Yield: 694 mg (82%). Calcd for $C_{68}H_{40}Cl_2N_4S_4Ir$: C, 62.61; H, 3.09; N, 4.30%. Found: C, 62.90; H, 3.15; N, 4.26%. ^1H NMR ($CDCl_3$, 400 MHz): δ (ppm) 9.14 (s, 4H, -Py), 7.81 (d, 4H, -Py), 7.70 (t, 8H, -Ph), 7.67 (d, 4H, -Ph), 7.23 (d, 4H, -Ph), 7.13 (t, 4H, -Ph), 7.03 (d, 4H, -Ph), 6.80 (d, 4H, -Ph), 6.73 (t, 4H, -Ph). ^{13}C NMR (100 MHz, $CDCl_3$) δ (ppm) 166.77, 163.25, 146.90, 143.26, 140.09, 136.81, 134.07, 130.85, 129.56, 127.56, 127.49, 126.96, 125.83, 125.25, 123.81, 121.37, 118.52.

Synthesis of the N^O-ancillary Schiff-base ligands HL^n (n = 1-3) from different salicylaldehyde derivatives

The N^O-ancillary Schiff-base ligands **HL^n** (n = 1-3) was synthesized from a rational condensation procedure of the equi-molar amount of aniline and each of the three salicylaldehyde derivatives (salicylaldehyde, *o*-vanillin or 3,5-di-*tert*-butyl-2-hydroxy-

benzaldehyde) as the literature.[5] For the **HL^1**: Yield: 93%. Calcd for $C_{13}H_{11}NO$: C, 79.17; H, 5.62; N, 7.10%. Found: C, 79.19; H, 5.58; N, 7.15%. ^{1}H NMR (DMSO-d_6, 400 MHz): δ (ppm) 13.11 (s, 1H, -OH), 8.97 (s, 1H, -CH=N), 7.67 (m, 1H, -Ph), 7.50-7.42 (m, 5H, -Ph), 7.33 (m, 1H, -Ph), 6.99 (m, 2H, -Ph).

For the **HL^2**: Yield: 89%. Calcd for $C_{14}H_{13}NO_2$: C, 73.99; H, 5.77; N, 6.16%. Found: C, 73.91; H, 5.85; N, 6.13%. ^{1}H NMR (DMSO-d_6, 400 MHz): δ (ppm) 13.26 (s, 1H, -OH), 8.96 (s, 1H, -CH=N), 7.46 (m, 4H, -Ph), 7.33 (t, 1H, -Ph), 7.25 (d, 1H, -Ph), 7.14 (d, 1H, -Ph), 6.92 (t, 1H, -Ph), 3.83 (s, 3H, -OMe).

For the **HL^3**: Yield: 92%. Calcd for $C_{21}H_{27}NO$: C, 81.51; H, 8.79; N, 4.53%. Found: C, 81.55; H, 8.76; N, 4.55%. ^{1}H NMR (DMSO-d_6, 400 MHz): δ (ppm) 13.96 (s, 1H, -OH), 8.99 (s, 1H, -CH=N), 7.50 (d, 1H, -Ph), 7.45 (m, 4H, -Ph), 7.40 (d, 1H, -Ph), 7.32 (t, 1H, -Ph), 1.43 (s, 9H, -C$(CH_3)_3$), 1.29 (s, 9H, -C$(CH_3)_3$).

X-ray crystallography

Single crystals for the Ir(III)-complexes [Ir(iqbt)$_2$(L^1)] (**1**), [Ir(iqbt)$_2$(L^2)]·CH_2Cl_2 (**2**·CH_2Cl_2) and [Ir(iqbt)$_2$(L^3)]·CH_2Cl_2 (**3**·CH_2Cl_2) of suitable dimensions were mounted onto thin glass fibers. All the intensity data were collected on a Bruker APEX-II CCD diffractometer (Mo-Kα radiation and λ = 0.71073 Å) in Φ and ω scan modes. Structures were solved by Direct methods followed by difference Fourier syntheses, and then refined by full-matrix least-squares techniques against F^2 using SHELXTL.[6] All other non-hydrogen atoms were refined with anisotropic thermal parameters. Absorption corrections were applied using SADABS.[7]

All hydrogen atoms were placed in calculated positions and refined isotropically using a riding model. Crystallographic data, relevant atomic distances and bond angles for the Ir(III)-complexes $[Ir(iqbt)_2(L^1)]$ (**1**), $[Ir(iqbt)_2(L^2)]\cdot CH_2Cl_2$ (**2**$\cdot CH_2Cl_2$) and $[Ir(iqbt)_2(L^3)]\cdot CH_2Cl_2$ (**3**$\cdot CH_2Cl_2$) are presented in **Tables S1-2**, respectively. The CCDC numbers 2098731-2098733 for the Ir(III)-complexes $[Ir(iqbt)_2(L^1)]$ (**1**), $[Ir(iqbt)_2(L^2)]\cdot CH_2Cl_2$ (**2**$\cdot CH_2Cl_2$) and $[Ir(iqbt)_2(L^3)]\cdot CH_2Cl_2$ (**3**$\cdot CH_2Cl_2$), respectively.

Electronic structure calculations

To gain further insight into the photo-physical and electrochemical characteristics of the Ir(III)-complexes, theoretical studies on their electronic structures were carried out by using density functional theory (DFT) and time-dependent DFT (TD-DFT) methods. Each of their molecular structures was optimized at the ground state (S_0) in the gas phase. DFT calculations were conducted with the popular B3LYP functional theory. The 6-31G (d,p) basis set was applied for C, H, N, O, S and Br atoms, while effective core potentials employed for Ir atom were based on a LanL2DZ basis set.[8-9] The energies of the excited states of the Ir(III)-complex were computed by TD-DFT based on all the ground-state (S_0) geometries. The contributions of fragments to the ‘‘holes’’ and ‘‘electrons’’ and Inter Fragment Charge Transfer (IFCT)[10] in the electronic excitation process were analyzed by the Ros and Schuit method[11] (C-squared population analysis method, SCPA) in the Multiwfn 3.8 program.[12] All calculations were carried out with Gaussian 09, Revision D.01 software package.[13] The electron density diagrams of molecular orbitals were obtained with the ChemOffice 2010 graphics program.

Cyclic voltammetry (CV) measurement

Electro-chemical measurements were made using a Princeton Applied Research model 2273A potentiostat at a scan rate of 100 mV s^{-1}. A conventional three-electrode configuration consisting of a glassy carbon working electrode, a Pt-sheet counter electrode, and a Pt wire reference electrode was used. The supporting electrolyte was 0.1 M tetrabutylammonium tetrafluoroborate ($[Bu_4N]BF_4$) in anhydrous MeCN. Ferrocene was added as a calibrant after each set of measurements, and all potentials reported are quoted with reference to the Fc^+/Fc couple. The oxidation (E_{ox}) and reduction (E_{red}) potentials were used to determine the HOMO and LUMO energy levels using Equations (2) and (3),[14] respectively,

$$E_{HOMO} = -(E_{OX}^{on} + 4.8)\ eV \qquad (2)$$

$$E_{LUMO} = E_{HOMO} + E_g^{OPT}\ eV \qquad (3)$$

where E_{OX}^{on} is the recorded onset oxidation potential of the complex, and E_g^{OPT} is the energy band gap estimated from the low-energy edge of the absorption spectra from the samples. The HOMO and LUMO energy levels for the other used materials were obtained from the literatures.[15]

Fabrication and testing of the NIR-PLEDs-1-3

Each of the **NIR-PLEDs-1-3** was fabricated on ITO (Indium tin oxide) coated glass substrates with a sheet resistance of 20 Ω per square. Patterned ITO coated glass substrates were

washed with acetone, detergent, D. I. water and isopropanol in an ultrasonic bath. After being exposed under oxygen plasma for 20 min, PEDOT:PSS from water solution was spin-coated (at 4800 rpm) on the substrate followed by drying in a vacuum oven at 130 °C for 30 min, giving a film of 50 nm in thickness. The chlorobenzene solution (30 mg/mL) of the mixture of PVK, OXD7 and one of the $[Ir(C^N)_2(N^O)]$-*bis*-heteroleptic Ir(III)-complexes **1**-**3** as the emitting layer (EML) was prepared under an N_2 atmosphere and spin-coated (at 4000 rpm) on the PEDOT:PSS layer with a thickness of 50 nm. The TmPyPB layer (45 nm) was thermally deposited onto the emitting layer. Finally, a thin layer (1 nm) of LiF followed by Al capping layer (100 nm) was deposited onto the substrate under vacuum (5×10^{-6} Pa). Current density-voltage (*J*-*V*) characteristics were collected using a Keithley 2400 source meter equipped with a calibrated silicon photodiode. The NIR EL irradiance (*R*) was measured through a PR735 SpectraScan spectrometer. The external quantum efficiency (η_{EQE}) of the NIR emission was obtained by measuring the irradiance in the forward direction and assuming the external emission profile to Lambertian.

References

1 J. H. Palmer, A. C. Durrell, Z. Gross, J. R. Winkler and H. B. Gray, *J. Am. Chem. Soc.*, 2010, **132**, 9230-9231.

2 G. R. Fu, H. Zheng, Y. N. He, W. T. Li, X.Q. Lü and H. S. He, *J. Mater. Chem. C*, 2018, **6**, 10589-10596.

3 S. Kesarkar, W. Mróz, M. Penconi, M. Pasini, S. Destri, M.Cazzaniga, D. Ceresoli, P. R. Mussini, C. Baldoli, U. Giovanella and A.Bossi, *Angew. Chem. Int. Ed.*, 2016, **55**, 2714-2718.

4 M. Nonoyama, *Bull. Chem. Soc. Jpn.,* 1979, **52**, 3749-3750.

5 Y. You, H. S. Huh, K. S. Kim, S. W. Lee, D. Kim and S. Y. Park, *Chem. Commun.,* 2008, 3998-4000.

6 G. M. Sheldrick, *SHELXL-97*, *Program for Crystal Structure Refinement*, University of 12 Göttingen, Göttingen, Germany, 1997.

7 G. M. Sheldrick, G. M. *SADABS*, University of Göttingen, Göttingen, Germany, 1996.

8 W. R. Wadt and P. J. Hay, *J. Chem. Phys.,* 1985, **82**, 284-298.

9 P. J. Hay and W. R. Wadt, *J. Chem. Phys.*, 1985, **82**, 299-310.

10 T. Lu, Multiwfn Manual, version 3.6 (dev), Section 3.21.1 and 3.21.8, available at http://sobereva.com/multiwfn.

11 P. Ros and G. C. A. Schuit, *Theor. Chim. Acta.,* 1966, **4**, 44-63.

12 T. Lu and F. W. Chen, *J. Comput. Chem.*, 2012, **33**, 580-592.

13 M. J. Frisch, G. W. Trucks, H. B. Schlegel, G. E. Scuseria, M. A. Robb, J. R. Cheeseman, G. Scalmani, V. Barone, B. Mennucci, G. A. Petersson, H. Nakatsuji, M. Caricato, X. Li, H. P. Hratchian, A. F. Izmaylov, J. Bloino, G. Zheng, J. L. Sonnenberg, M. Hada, M. Ehara, K. Toyota, R. Fukuda, J. Hasegawa, M. Ishida, T. Nakajima, Y. Honda, O. Kitao, H. Nakai, T. Vreven, J. A. Montgomery, Jr., J. E. Peralta, F. Ogliaro, M. Bearpark, J. J. Heyd, E. Brothers, K. N. Kudin, V. N. Staroverov, R. Kobayashi, J. Normand, K. Raghavachari, A. Rendell, J. C. Burant, S. S. Iyengar, J. Tomasi, M. Cossi, N. Rega, J. M. Millam, M. Klene, J. E. Knox, J. B.

Cross, V. Bakken, C. Adamo, J. Jaramillo, R. Gomperts, R. E. Stratmann, O. Yazyev, A. J. Austin, R. Cammi, C. Pomelli, J. W. Ochterski, R. L. Martin, K. Morokuma, V. G. Zakrzewski, G. A. Voth, P. Salvador, J. J. Dannenberg, S. Dapprich, A. D. Daniels, Ö. Farkas, J. B. Foresman, J. V. Ortiz, J. Cioslowski and D. J. Fox, Gaussian 09, Revision D.01, Gaussian, Inc., Wallingford CT, 2009.

14 H. Y. Chen, C. T. Chen and C. T. Chen, *Macromolecules,* 2010, **43**, 3613-3623.

15 E. Zysman-Colman, S. S. Ghosh, G. Xie, S. Varghese, M. Chowdhury, N. Sharma, D. B. Cordes, A. M. Z. Slawin and I. D. W. Samuel, *ACS Appl. Mater. & Interfaces,* 2016, **8**, 9247-9253.

Table S1 Crystallographic data and structure refinement for the Ir(III)-complexes **1**, **2**·CH_2Cl_2 and **3**·CH_2Cl_2.

Compound	**1**	**2**·CH_2Cl_2	**3**·CH_2Cl_2
Empirical formula	$C_{47}H_{30}N_3OS_2Ir$	$C_{49}H_{34}N_3O_2S_2Cl_2Ir$	$C_{56}H_{48}N_3OS_2Cl_2Ir$
Formula weight	909.06	1024.01	1106.19
Crystal system	Monoclinic	Monoclinic	Monoclinic
Space group	*P2(1)/c*	*P2(1)/c*	*P2(1)/c*
a/Å	17.559(2)	18.169(5)	10.792(4)
b/Å	15.5739(19)	14.436(4)	16.057(5)
c/Å	16.146(2)	16.263(5)	29.052(10)
α/°	90	90	90
β/°	96.022(2)	97.568(6)	96.608(7)
γ/°	90	90	90
V/Å^3	4390.7(10)	4228(2)	5001(3)
Z	4	4	4
ρ/g·cm^{-3}	1.375	1.609	1.469
Crystal size/mm	0.28× 0.29 × 0.25	0.29× 0.30× 0.24	0.30× 0.34× 0.28
μ(Mo-Kα)/mm^{-1}	3.172	3.427	2.902
Data/restraints/paramet	8250/0/487	8497/0/532	10493/9/586
Quality-of-fit indicator	1.098	0.958	0.922
No. unique reflections	8250	8497	10493
No. observed reflections	22565	22897	27907
Final *R* indices [*I*> 2σ(*I*)]	R_1 = 0.0567	R_1 = 0.0565	R_1 = 0.0902
	wR_2 = 0.1702	wR_2 = 0.1123	wR_2 = 0.1838
R indices (all data)	R_1 = 0.0804	R_1 = 0.1194	R_1 = 0.2547
	wR_2 = 0.1864	wR_2 = 0.1368	wR_2 = 0.2590

Table S2 The relevant bond lengths (Å) and bond angles (°) for the Ir(III)-complexes **1**, **2**·CH_2Cl_2 and **3**·CH_2Cl_2.

Compound	**1**	**2**·CH_2Cl_2	**3**·CH_2Cl_2
Ir(1)-C(7)	2.015(9)	1.991(9)	2.037(15)
Ir(1)-C(24)	2.008(8)	1.997(8)	1.918(18)
Ir(1)-N(1)	2.052(7)	2.043(7)	2.052(13)
Ir(1)-N(2)	2.055(7)	2.066(7)	2.053(14)
Ir(1)-N(3)	2.167(7)	2.131(6)	2.129(12)
Ir(1)-O(1)	2.115(6)	2.120(6)	2.095(11)
N(1)-Ir(1)-C(7)	78.5(3)	77.8(3)	77.9(6)
N(2)-Ir(1)-C(24)	78.7(3)	78.7(3)	78.8(7)
O(1)-Ir(1)-N(3)	88.0(2)	88.1(2)	86.4(5)

Table S3 The photophysical properties of the C_1-symmetric [Ir(C^N)$_2$(N^O)-*bis*-heteroleptic Ir(III)-complexes **1**-**3** in degassed CH_2Cl_2 solution at room temperature

Comp.	Absorption[a]	Emission[a]						Energy level	
	λ_{abs}[nm]	λ_{ex}[nm]	λ_{em}[nm]	τ [μs]	Φ_{PL}	k_r[b](10^5 s^{-1})	k_{nr}[b](10^6 s^{-1})	HOMO[c][eV]	LUMO[c][eV]
1	292, 365, 403, 539;	550	708, 768(sh)	0.74	0.19	2.6	1.1	-5.32 (-4.77)	-3.23 (-1.93)
2	280, 363, 403, 542;	558	706, 766(sh)	0.79	0.13	1.6	1.1	-5.24 (-4.72)	-3.14 (-1.89)
3	292, 363, 408,538;	544	708, 768(sh)	0.75	0.17	2.3	1.1	-5.26 (-4.79)	-3.17 (-1.95)

[a]Measured in degassed CH_2Cl_2 solution;

[b]$k_r = \Phi_{PL}/\tau$, $k_{nr} = (1 - \Phi_{PL})/\tau$;

[c]HOMO and LUMO levels are obtained from electrochemical determination and theoretical calculations, respectively.

Table S4 Frontier orbital energy and electron density distribution for the *bis*-heteroleptic Ir(III)-complexes **1-3** on the basis of their optimized S_0 geometries

Complex	MO	Contribution of metal d_π orbitals and π orbitals			
		Ir	Iqbt-1	Iqbt-2	N^O
1	LUMO+2	1.77	1.31	1.02	95.90
	LUMO+1	4.76	69.04	24.01	2.19
	LUMO	5.14	24.55	68.56	1.75
	HOMO	23.60	38.57	35.66	2.17
	HOMO-1	13.07	1.98	2.29	82.66
	HOMO-2	0.57	49.93	48.44	1.05
2	LUMO+2	1.92	1.04	1.05	95.99
	LUMO+1	4.79	68.65	24.69	1.86
	LUMO	5.12	25.22	67.87	1.78
	HOMO	20.63	31.82	27.10	20.45
	HOMO-1	10.54	8.33	9.67	71.47
	HOMO-2	0.47	49.39	48.91	1.22
3	LUMO+2	1.75	0.86	1.00	96.40
	LUMO+1	4.70	40.19	53.30	1.81
	LUMO	5.17	52.68	40.63	1.52
	HOMO	23.93	36.70	36.36	3.02
	HOMO-1	9.75	2.24	1.25	86.76
	HOMO-2	5.87	20.67	3.95	69.51

Table S5 Frontier orbital energy and electron density distribution for the *bis*-heteroleptic Ir(III)-complexes **1-3** on the basis of their optimized T_1 geometries

complex	MO	Contribution of metal d_π orbitals and π orbitals			
		Ir	Iqbt-1	Iqbt-2	N^O
1	LUMO+2	1.60	0.78	1.08	96.55
	LUMO+1	4.78	2.68	91.09	1.44
	LUMO	6.18	88.84	2.75	2.24
	HOMO	20.28	55.47	22.68	1.57
	HOMO-1	11.54	2.63	1.98	83.84
	HOMO-2	1.77	32.25	64.24	1.75
2	LUMO+2	1.79	1.17	1.00	96.04
	LUMO+1	5.34	24.90	67.88	1.88
	LUMO	5.50	67.28	25.37	1.86
	HOMO	21.71	32.97	42.35	2.96
	HOMO-1	7.03	2.34	1.24	89.40
	HOMO-2	0.56	51.70	46.33	1.42
3	LUMO+2	1.59	0.69	0.81	96.91
	LUMO+1	4.77	3.07	91.01	1.15
	LUMO	6.13	88.66	3.08	2.12
	HOMO	20.25	57.27	20.51	1.97
	HOMO-1	1.76	31.55	65.11	1.58
	HOMO-2	19.58	36.58	33.01	10.83

Table S6 The calculated orbital transition analyses for the *bis*-heteroleptic Ir(III)-complexes **1-3** by TD-DFT calculations with the IFCT analyses at the B3LYP level

Comp.	state	λ (nm)	E (eV)	oscillator (f)	transition (contrib.)	assignment			
1	$S_0 \rightarrow S_1$	546	2.2708	0.0182	HOMO → LUMO (95.4%)	^{1}ILCT 33.95%	^{1}MC 1.21%	^{1}MLCT 22.39%	^{1}LMCT 3.93%
						^{1}LLCT 38.52%			
	$S_0 \rightarrow T_1$	713	1.7386	0.0000	HOMO → LUMO (75.8%); HOMO-2 → LUMO+1 (12.7%); HOMO-2 → LUMO (5.8%)	^{3}ILCT 44.33%	^{3}MC 1.00%	^{3}MLCT 18.74%	^{3}LMCT 4.07%
						^{3}LLCT 31.86%			
	$T_1 \rightarrow S_0$	923	1.3435	0.0000	HOMO → LUMO (84.6%); HOMO-2 → LUMO (11.6%)	^{3}ILCT 70.18%	^{3}MC 0.95%	^{3}MLCT 14.50%	^{3}LMCT 5.22%
						^{3}LLCT 9.15%			
2	$S_0 \rightarrow S_1$	548	2.2645	0.0154	HOMO → LUMO (91.3%)	^{1}ILCT 26.08%	^{1}MC 1.05%	^{1}MLCT 19.58%	^{1}LMCT 4.05%
						^{1}LLCT 49.25%			
	$S_0 \rightarrow T_1$	713	1.7379	0.0000	HOMO → LUMO (60.4%); HOMO-1→ LUMO (16.1%); HOMO-2 → LUMO+1 (13.3%); HOMO-2 → LUMO (5.0%)	^{3}ILCT 43.58%	^{3}MC 1.00%	^{3}MLCT 18.75%	^{3}LMCT 4.07%
						^{3}LLCT 32.60%			
	$T_1 \rightarrow S_0$	803	1.5446	0.0000	HOMO → LUMO (76.8%), HOMO-2→ LUMO+1 (13.8%)	^{3}ILCT 40.85%	^{3}MC 1.01%	^{3}MLCT 17.47%	^{3}LMCT 4.46%
						^{3}LLCT 36.22%			
3	$S_0 \rightarrow S_1$	545	2.2754	0.0062	HOMO → LUMO (92.5%)	^{1}ILCT 33.11%	^{1}MC 1.21%	^{1}MLCT 22.25%	^{1}LMCT 3.94%
						^{1}LLCT 39.49%			
	$S_0 \rightarrow T_1$	712	1.7418	0.0000	HOMO → LUMO (74.7%); HOMO-2 → LUMO+1 (16.8%)	^{3}ILCT 36.28%	^{3}MC 1.00%	^{3}MLCT 18.64%	^{3}LMCT 4.09%
						^{3}LLCT 40.01%			
	$T_1 \rightarrow S_0$	920	1.3479	0.0000	HOMO → LUMO (85.3%); HOMO-2 → LUMO (11.0%)	^{3}ILCT 71.03%	^{3}MC 0.93%	^{3}MLCT 14.22%	^{3}LMCT 5.21%
						^{3}LLCT 8.62%			

Table S7 The transition dipole moments $\Delta\mu$ comparison for the *bis*-heteroleptic Ir(III)-complexes **1-3** with upon DFT calculations based on their corresponding optimized T_1 and S_0 states

Complex	State	*x*	*y*	*z*	$\left\|\vec{\mu}\right\|$ (D)	ϑ (°)	$\left\|\Delta\vec{\mu}\right\|$ (^{1}T-^{0}S) (D)
1	S_0	-1.1908	1.9043	1.6842	2.81	49	2.35
	T_1	1.0377	1.4109	2.2507	2.85		
2	S_0	0.2747	1.8456	-1.5519	2.43	2	0.56
	T_1	0.2293	1.4573	-1.1495	1.87		
3	S_0	-0.3147	-1.6097	-2.1256	2.68	60	3.01
	T_1	1.1633	0.9072	-2.8767	3.23		

Table S8 Summarized coefficients (maximum ordinary coefficient k_o^{max}, maximum extraordinary coefficient k_e^{max}), θ' angles between the transition dipole moment vector and the direction vertical to the substrate, order parameters (*S*), and horizontal dipole ratios ($h/(h+v)$) of the spin-coated **EMLs-1-3** for the **NIR-PELDs-1-3** composed of PVK-OXD7 (65:30, wt%) as the host and each of the Ir(III)-complexes **1-3** as the dopant at 5 wt% doping level.

EML	k_e^{max} (λ)	k_o^{max} (λ)	θ' (°)	S[a]	$h/(h+v)$[b]
PVK:OXD7:**1** (65:30:5; wt%)	0.416 (240 nm)	0.673 (205 nm)	60.93	-0.146	0.763
PVK:OXD7:**2** (65:30:5; wt%)	0.506 (238 nm)	0.532 (220 nm)	55.41	-0.017	0.678
PVK:OXD7:**3** (65:30:5; wt%)	0.486 (233 nm)	0.715 (217 nm)	59.76	-0.120	0.746

[a] $S = \frac{k_e^{max} - k_o^{max}}{k_e^{max} + 2k_o^{max}} = \frac{3cos^2\theta' - 1}{2}$

[b] $\frac{h}{h+v} = \frac{2(1-S)}{3}$

Scheme S1 Reaction scheme for the synthesis of the [Ir(C^N)$_2$(N^O)-*bis*-heteroleptic iridium(III)-complexes **[Ir(iqbt)$_2$(L^n)]** (n = 1-3, **1-3**)

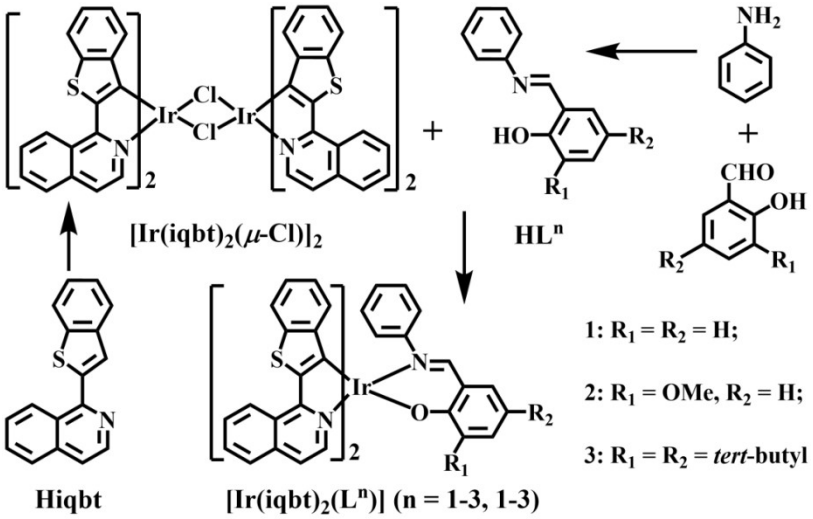

Figure S1 The ^{1}H NMR spectra of the chloride-bridged dimer intermediate $[Ir(iqbt)_2(\mu\text{-}Cl)]_2$ and the $[Ir(C^N)_2(N^O)]$-*bis*-heteroleptic Ir(III)-complexes $[Ir(iqbt)_2(L^n)]$ (n = 1-3, **1-3**) in $CDCl_3$ at room temperature.

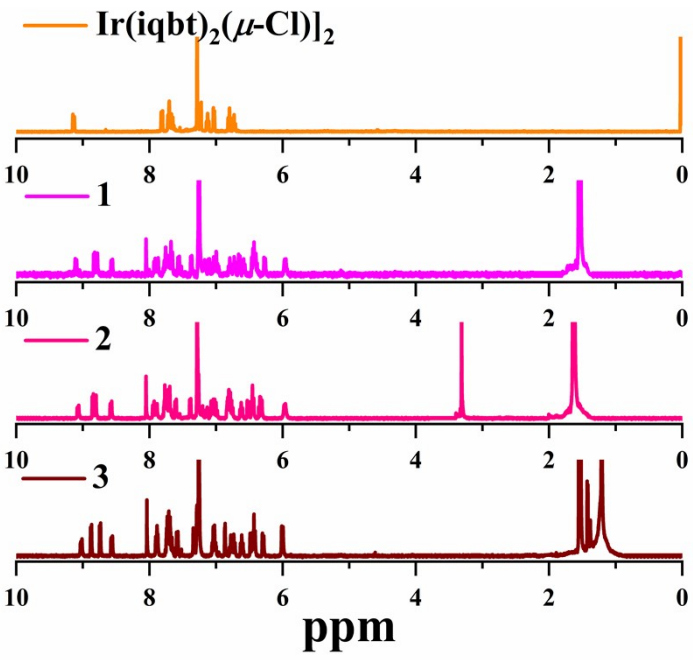

Figure S2 The ^{13}C NMR spectra of the chloride-bridged dimer intermediate $[Ir(iqbt)_2(\mu\text{-}Cl)]_2$ and the $[Ir(C^N)_2(N^O)]$-*bis*-heteroleptic Ir(III)-complexes $[Ir(iqbt)_2(L^n)]$ (n = 1-3, **1-3**) in $CDCl_3$ at room temperature.

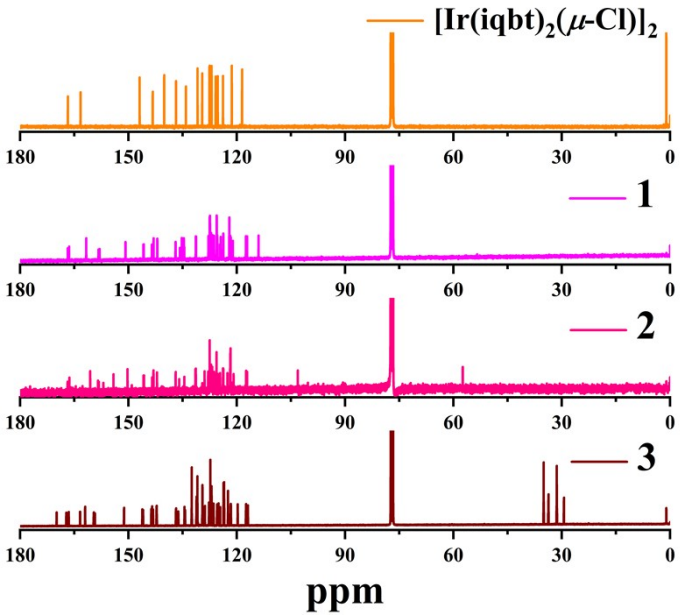

Figure S3 The ESI-MS data of the $[Ir(C^N)_2(N^O)]$-*bis*-heteroleptic Ir(III)-complexes $[Ir(iqbt)_2(L^n)]$ (n = 1-3, **1-3**) in CH_2Cl_2 at room temperature.

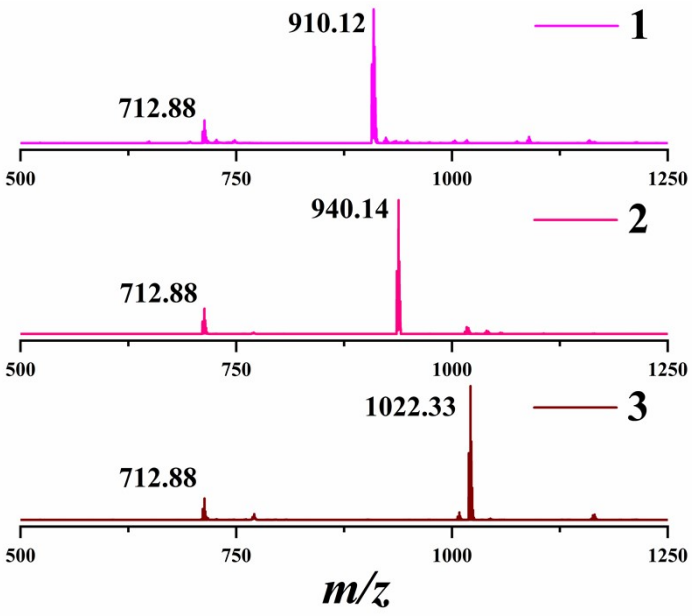

Figure S4 The ^{1}H NMR spectra for the HC^N main ligand **Hiqbt** and the N^OH-ancillary ligand **HL^{n}** (n = 1-3) at room temperature.

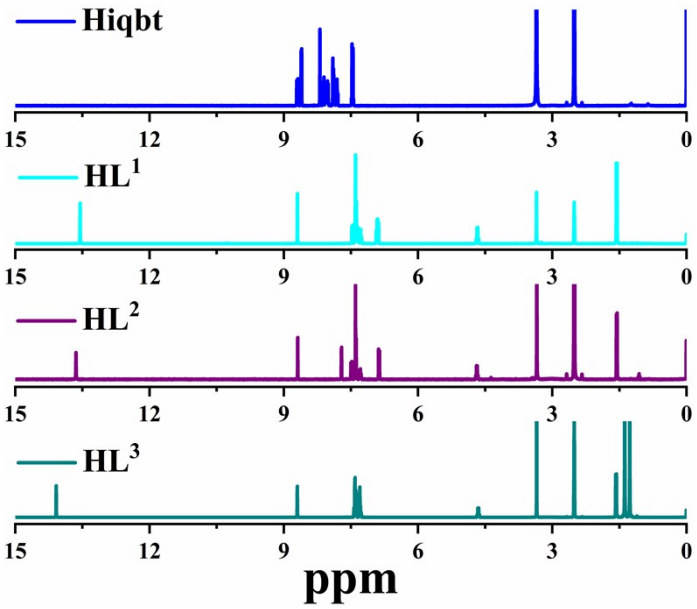

Figure S5 TG (thermogravimetric analysis) curves for the *bis*-heteroleptic Ir(III)-complexes **1**-**3**

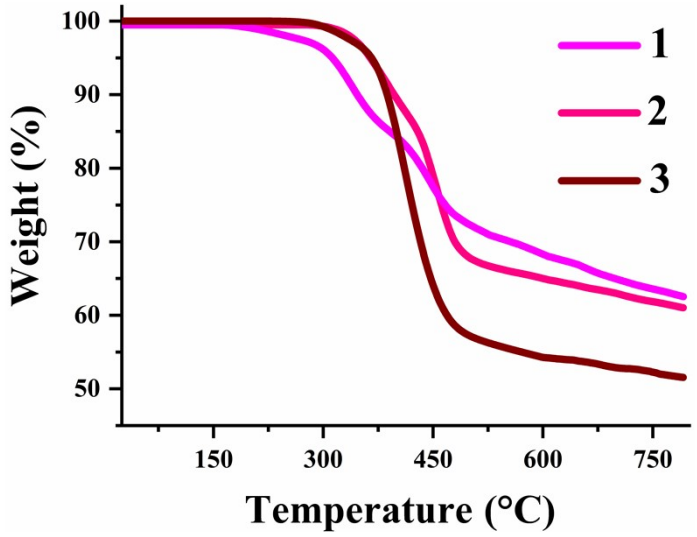

Figure S6 The normalized emission spectra (λ_{ex} = 550 nm (**1**), 558 nm (**2**) or 544 nm (**3**)) of the *bis*-heteroleptic Ir(III)-complex [Ir(iqbt)$_2$(L^n)] (n = 1-3, **1-3**) in different solvents at room temperature.

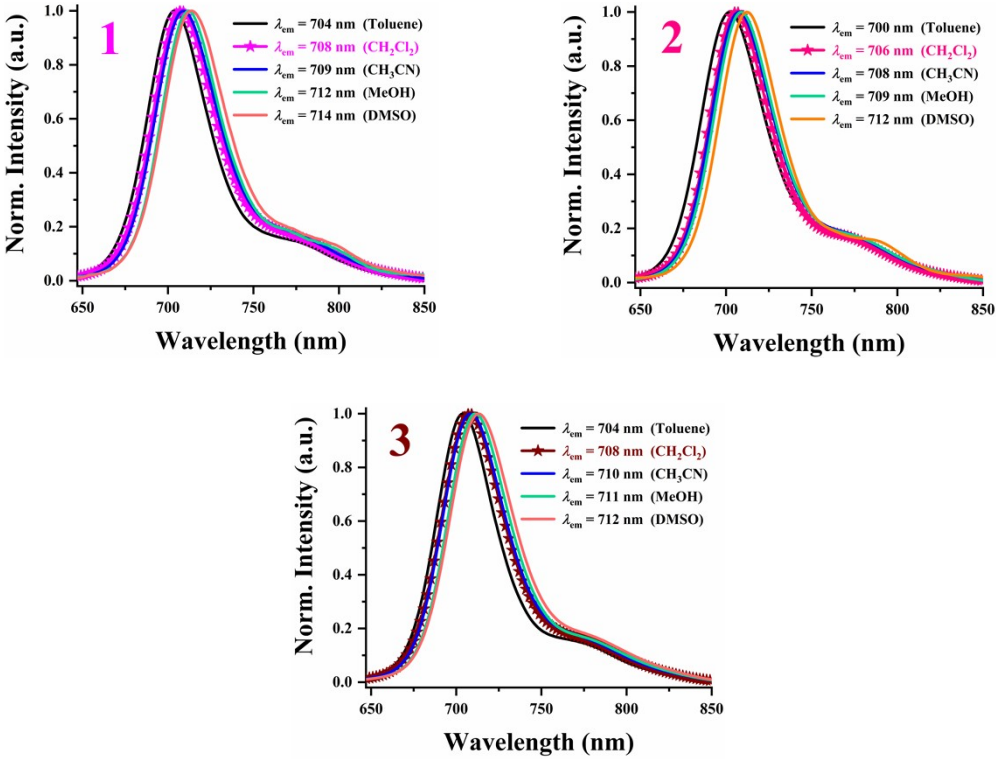

Figure S7 The normalized emission spectra (λ_{ex} = 365 nm) for the *bis*-heteroleptic Ir(III)-complexes [Ir(iqbt)$_2$(L^n)] (n = 1-3, **1-3**) in crystalline powder at room temperature.

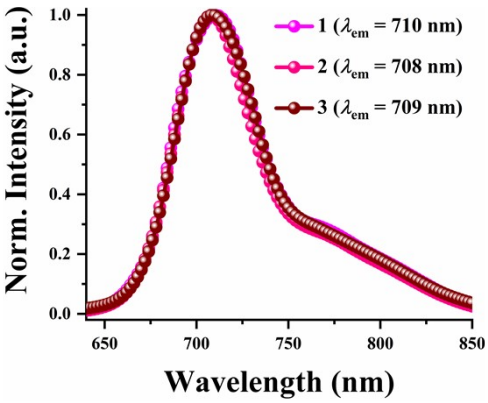

Figure S8 The normalized UV-visible absorption spectra of the HC^N main ligand **Hiqbt** and the N^OH-ancillary ligand **HL^n** (n = 1-3) in degassed CH_2Cl_2 solutions at room temperature.

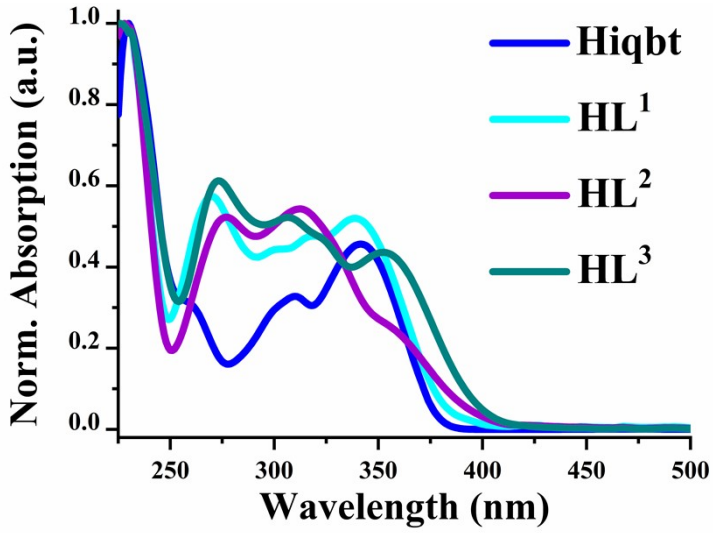

Figure S9 The normalized excitation and emission spectra of the HC^N main ligand **Hiqbt** and the N^OH-ancillary ligand **HL^n** (n = 1-3) in degassed CH_2Cl_2 solutions at room temperature.

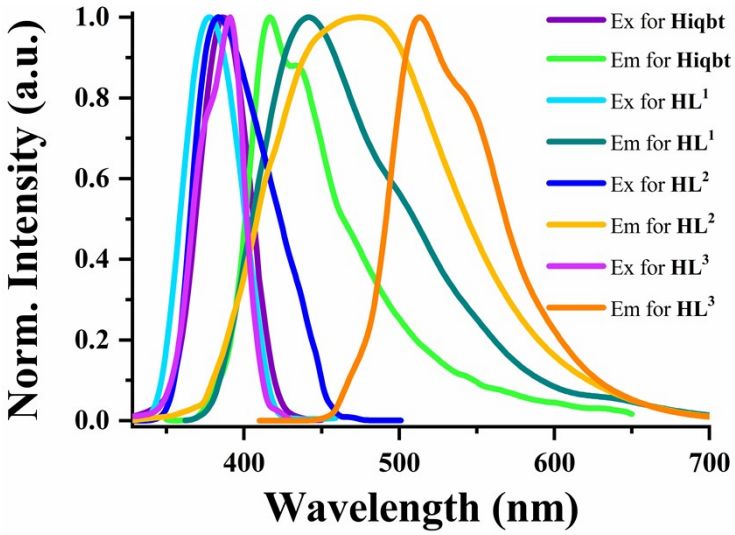

Figure S10 The PXRD (powder X-ray diffraction) curves of PVK, the *co*-host of PVK-OXD7 (65:30; weight ratio) and the doped films (PVK:OXD7:**1**/**2**/**3** (65:30:5; wt%)), respectively.

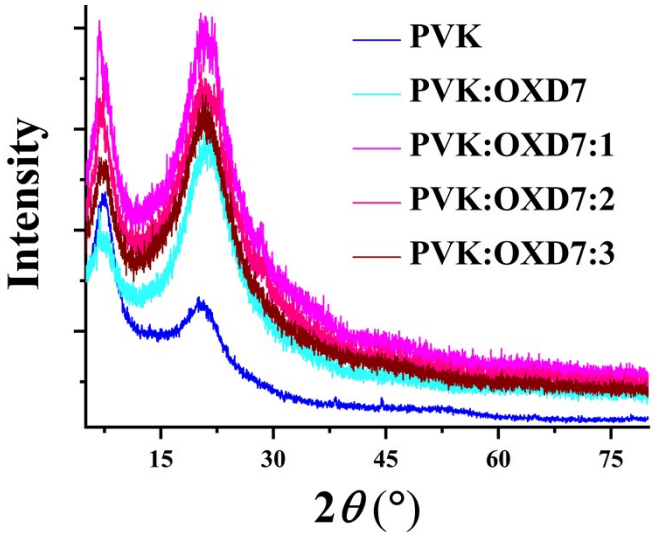

Figure S11 The AFM (atomic force microscopy) pictographs of films with the pure PVK (a), the *co*-host of PVK-OXD7 (65:30; weight ratio) (b) and the doped EMLs of PVK:OXD7:Ir(III)-complex **1**/**2**/**3** (65:30:5; wt%) (c-e) through spin-coating, respectively.

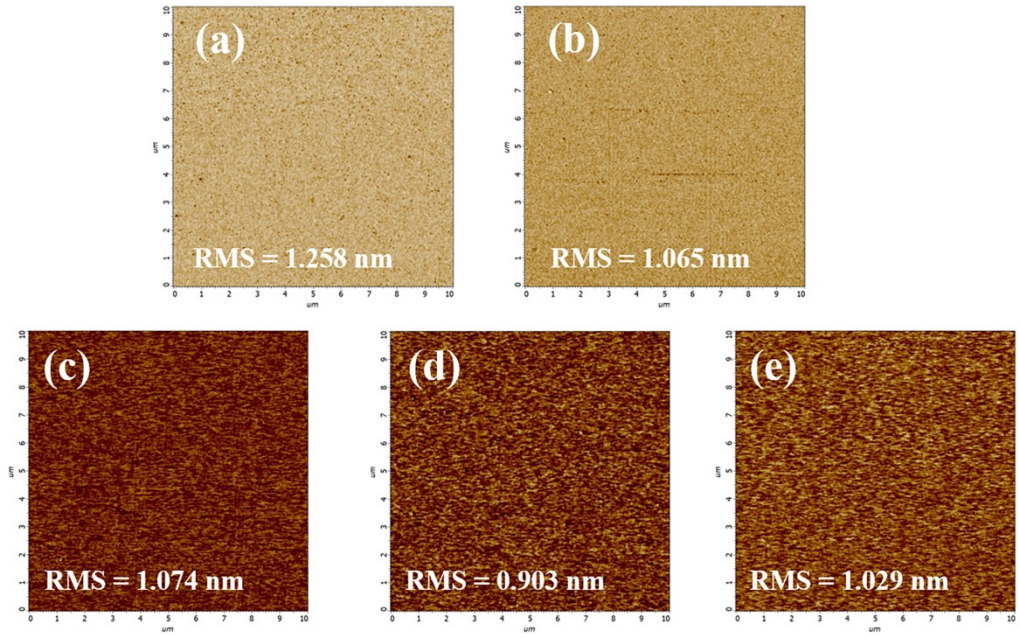

Figure S12 The normalized emission spectra (λ_{ex} = 365 nm) for the doped EML films consisting of PVK:OXD7:Ir(III)-complex **1**/**2**/**3** (65:30:5; wt%) at room temperature.